The forgotten land use class

Mapping of fallow fields across the Sahel using Sentinel-2

Tong, Xiaoye; Brandt, Martin; Hiernaux, Pierre; Herrmann, Stefanie; Rasmussen, Laura Vang; Rasmussen, Kjeld; Tian, Feng; Tagesson, Torbern; Zhang, Wenmin; Fensholt, Rasmus

Published in:
Remote Sensing of Environment

DOI:
10.1016/j.rse.2019.111598

2020

Document Version:
Peer reviewed version (aka post-print)

Please cite as: Tong, X., Brandt, M., Hiernaux, P., Herrmann, S., Rasmussen, L.V., Rasmussen, K., Tian, F., Tagesson, T., Zhang, W., & Fensholt, R. (2020). The forgotten land use class: Mapping of fallow fields across the Sahel using Sentinel-2. Remote Sensing of Environment, 239, 111598

The forgotten land use class: mapping of fallow fields across the Sahel using Sentinel-2

Xiaoye Tong [a], Martin Brandt [a], Pierre Hiernaux [b], Stefanie Herrmann [c], Laura Vang Rasmussen [d], Kjeld Rasmussen [a], Feng Tian [e], Torbern Tagesson [a,e], Wenmin Zhang [f], Rasmus Fensholt [a]

[a] Department of Geosciences and Natural Resource Management (IGN), University of Copenhagen, 1350 Copenhagen, Denmark

[b] Pastoc, 30 chemin de Jouanal, 82160, Caylus, France

[c] The University of Arizona, Tucson, AZ 85719, USA

[d] Department of Forest and Conservation Sciences, University of British Columbia, 3609 - 2424 Main Mall, Vancouver, BC V6T 1Z4

[e] Department of Physical Geography and Ecosystem Sciences, Lund University, Sölvegatan 12, 223 62 Lund, Sweden

[f] School of Geography Science, Nanjing Normal University, Nanjing 210023, China

Abstract

Remote sensing-derived cropland products have depicted the location and extent of agricultural lands with an ever increasing accuracy. However, limited attention has been devoted to distinguishing between actively cropped fields and fallowed fields within agricultural lands, and in particular so in grass fallow systems of semi-arid areas. In the Sahel, one of the largest dryland regions worldwide, crop-fallow rotation practices are widely used for soil fertility regeneration. Yet, little is known about the extent of fallow fields since fallow is not explicitly differentiated within the cropland class in any existing remote sensing-based land use/cover maps, regardless of the spatial scale. With a 10 m spatial resolution and a 5-day revisit frequency, Sentinel-2 satellite imagery made it possible to disentangle agricultural land into cropped and fallow fields, facilitated by Google Earth Engine (GEE) for big data handling. Here we produce the first Sahelian fallow field map at a 10 m resolution for the baseline year 2017, accomplished by designing a remote sensing driven protocol for generating reference data for mapping over large areas. Based on the 2015 Copernicus Dynamic Land Cover map at 100 m resolution, the extent of fallow fields in the cropland class is estimated to be 63% (403 617 km^2) for the Sahel in 2017. Similar results are obtained for five contemporary cropland products, with fallow fields occupying 57-62% of the cropland area. Yet, it is noted that the total estimated area coverage depends on the quality of the different cropland products. The share of cropped fields within the Copernicus cropland area is found to be higher in the arid regions (200-300 mm rainfall) as compared to the semi-arid regions (300-600 mm rainfall). The woody cover fraction within cropped and fallow fields is found to have a reversed pattern between arid (higher woody cover in cropped fields) and semi-arid (higher woody cover in fallow fields) regions. The method developed, using cloud-based Earth Observation (EO) data and computation on the GEE platform, is expected to be reproducible for mapping the extent of fallow fields across global croplands. Future applications based on multi-year time series is expected to improve our understanding of crop-fallow rotation dynamics in grass fallow systems being key in teasing apart how cropland intensification and expansion affect environmental variables, such as soil fertility, crop yields and local livelihoods in low-income regions such as the Sahel. The mapping result can be visualized via a web viewer (https://buwuyou.users.earthengine.app/view/fallowinsahel).

Keywords: fallow fields, cropland, satellite image time series, land use/cover mapping, Sentinel-2, drylands, Sahel

1. Introduction

Natural regeneration from multi-year grass and bush fallowing is an integral part of rain-fed cultivation systems across the Sahel, as fallowing is one of the land management strategies to restore soil fertility when access to livestock manure or chemical fertilizers is limited (Gandah et al., 2003; Serpantié et al., 2001; Samaké et al., 2005). While intrinsically linked with the land use/land cover category "cropland", Sahelian fallow fields are arguably quite distinct from cropped fields in form and function. Fallow fields are characterized by a continuous herbaceous vegetation cover (an increasing cover as a function of the number of years left for fallow), whereas cropped fields show a dominant fraction of bare soil with an interspersed sparse cereal crop cover (Fig. 1b and 1c). Differing from seasonal cultivated and fallowed cropland systems as mapped by Wallace et al. (2017) and Wu et al. (2014), the fallowing in Sahelian cultivation systems typically lasts for two to five years, to retain satisfactory physical and chemical soil fertility conditions. In fallowing years, Sahelian fallow fields do not generate crop yields, and hence should be mapped as a separate category when mapping cropland areas on an annual basis. Moreover, temporal changes in crop-fallow cycles can be indicative of changes in a range of environmental and socio-economic parameters. For example, shorter rotation cycles might be associated with population pressure and declining soil fertility (De Ridder et al., 2004; De Rouw and Rajot, 2004). A distinction between fallow and cropped fields is thus important for assessments related to food security, the provisioning of ecosystem services, and land degradation, etc. Yet, this distinction has so far only been adopted when assessing the area cover of fallow and croplands at the plot scale (Hiernaux et al., 2009; Tong et al., 2017).

Remote sensing techniques have long been used for land use/cover classification, and in particular so for applications of mapping agricultural lands (Bégué et al., 2018). Specifically, repeated observations offered by multi-temporal remote sensing can capture the different seasonal cycles of vegetation types, thereby enabling phenology-based classifications (Dong et al., 2016; Zhong et al., 2016). Seasonal cultivated and fallow cropland mapping in the US has been conducted using e.g. MODIS or VHR-based automated cropland classification algorithm (Wallace et al., 2017; Wu et al., 2014; Xie et al., 2007). Yet, in spite of the unprecedented advances to monitor the land surface using remote sensing techniques in recent decades, Sahelian grass fallow land has not been mapped separately from croplands in any of the existing global and regional land cover products originating from various Earth Observation (EO) datasets, including Landsat, MODIS (Moderate Resolution Imaging Spectroradiometer) and PROBA-V (Project for On-Board Autonomy-Végétation) (Chen et al., 2015; Lambert et al., 2016; Xiong et al., 2017; Copernicus Global Land Service, 2019; Bégué et al., 2014). Tong et al. (2017) found clear differences between the seasonal patterns of cropped and fallow fields in western Niger using MODIS time series and employed a sub-pixel method to map fallow percentage at a 250 m resolution. However, Sahelian cropped and fallow fields are not only fragmented in distribution but also small in size (up to only a few hectares) (Raynaut 1998; Fritz et al., 2015; Mortimore et al., 2001). The sub-pixel approach developed in Tong et al. (2017) did not resolve the spatial delineation of heterogeneous field objects at a sufficient scale. Therefore, a scalable approach is needed to allow a direct mapping of fallow fields at a fine resolution covering large spatial extents like the Sahel.

Fallow fields in Sahelian croplands (Fig. 1a) can be very different from cropped fields, from a remote-sensing perspective. Firstly, from a spectral perspective, fallow fields in the Sahel are generally greener (higher NDVI (Normalized Difference Vegetation Index) values) than cropped fields during the growing season (Tong et al., 2017). This is caused by the characteristics of the traditional cropping systems with low inputs of chemical fertilizer and cropping practices such as land clearing, ploughing, sowing in distant pockets, repeated weeding, and harvest activities in cropped fields that significantly reduce herbaceous vegetation cover on actively cropped fields. Contrastingly, fallow fields gradually develop into a continuous coverage of herbaceous and growing shrub vegetation during consecutive years of fallow (Achar et al., 2001). Secondly, from a temporal perspective, fallow and cropped fields have different seasonal features with fallow fields showing an advanced senescence as compared to cropped fields (Fig.1d) (Tong et al., 2017). Consequently, the challenges in separating fallow fields from croplands, relate to the following: (i) imagery needs to be acquired at a certain time of the year for optimally capturing the seasonal NDVI differences between crops and fallow, thus requiring high temporal resolution. For the Sahel, the optimal time window varies along a north-south gradient but is located around the dry-down period of the growing season; (ii) The small field size typical of the smallholder agriculture presented in the region simultaneously requires optical satellite sensor systems that have a high spatial resolution; and (iii) training samples of cropped and fallow fields adequately representing the heterogeneous landscapes are needed. As traditional satellite systems have only fulfilled one of the first two criteria, the Sentinel-2 constellation of two identical Multispectral Imager sensor (MSI) systems has opened a new avenue for mapping fallow fields at the regional scale by combining a high spatial resolution (10 m for the visible and near-infrared (NIR) wavelengths) with a high temporal resolution (5-day revisit time). The Sentinel-2 sensor offers a significant improvement over the Landsat TM, ETM+ and OLI sensors in relation to aspects (i) and (ii) mentioned above.

Ground data is paramount for land cover classification by providing accurate training inputs and validating output classes. The collection of ground data is however laborious and time-consuming, in particular when mapping large areas. Increasing efforts are being devoted to gathering common reference data for both training and validation purposes on global land cover products (Fritz et al., 2012), with a specific focus on Africa (Tsendbazar et al., 2018b). Yet ground reference data distinguishing Sahelian cropland and fallow fields is still missing. In the absence of such ground observations, manually digitized reference data using satellite imagery guided by expert knowledge is a viable alternative, but is only feasible in the form of a rather sparse distribution across the region. Also, an uneven distribution of reference data can result in an insufficient representation of within-class variability of individual land use/cover classes across space (Cracknell and Reading, 2014). It is thus critical to automate the reference data generation for fallow and cropped fields, with adequate spatial distribution representing the local characteristics of fields.

In this study, we are aiming to map cropped and fallow land patches (hereafter referred as fallow and cropped fields) across the entire Sahel at a 10 m spatial resolution. Google Earth Engine (GEE) and a Random Forest classifier are used to process the Sentinel-2 imagery archived from 2017 to detect the spatial extent of fallow fields within croplands mapped by Copernicus Dynamic Land Cover map at 100 m resolution (CGLS-LC100) (Copernicus Global Land Service, 2019). CGLS-

LC100 has been reported to show higher classification accuracy for the Sahel as compared to other global land cover maps (Tsendbazar et al., 2018a). A comprehensive reference dataset is generated across Sahelian fields using a two-step automated approach. The Sahel-wide map of cropped/fallow fields in 2017 is then analyzed in relationship to rainfall and woody cover. Finally, fallow fields were also mapped in five additional contemporary cropland products (ESA CCI 300 m 2015, GlobeLand30 2010, GFSAD30 2015, Lambert et al., 2016 and Tappan et al., 2016) to estimate the extent of Sahelian fallow fields encompassed in the current state-of-the-art mapping of croplands.

2. Materials and methods

2.1 Study area

The study area covers Sahelian croplands as defined by the CGLS-LC100 land cover map from 2015 (Fig. 1a). The Sahel is an arid and semi-arid region between the Sahara in the north and the sub-humid tropical savannas in the South. It stretches from Senegal-Mauritania in the West to Sudan-Eritrea in the East, including parts of Mali, Burkina Faso, Niger, Nigeria, Chad and Southern Sudan. Most crop systems are rain-fed (93% of all agricultural systems) with pearl millet and sorghum being the main crops (Sultan et al., 2013; Rasmussen et al., 2012a). Livelihoods are strongly linked to the exploitation of natural resources, which makes the rural population particularly susceptible to climate variability, often having deleterious effects on the agricultural production (Cooper et al., 2008; Sheffield et al., 2014; Douxchamps et al., 2016).

Common farming practices to maintain or improve crop yields include soil tillage, crop residue management, manuring and fertilizer application, crop association or rotation, choice of drought-resistant breeds, and fallowing (Hiernaux and Turner 2002). The application of mineral fertilizers is less widespread because of the insufficient economic responses following their application (Rasmussen et al., 2012a). The farmers normally decide before the onset of the rain which areas to keep under fallow when the sowing takes place. Yet, in years with low rainfall which is detrimental to total yields, or badly distributed rainfall with long dry spells farmers might also decide after sowing to concentrate the weeding in specific areas of their field and leave the remaining areas fallow (Rasmussen et al., 2012b). The herbaceous vegetation in fallow areas then remains unmanaged, and the subsequent growth of vegetation depends largely on the rainfall. Grazing activities, however, might cause a reduction of the vegetation in fallow fields. The extent of fallowing may, on the one hand, be constrained by limited access to cropland by some families aggravated by the context of steady rural population growth (van Vliet et al., 2013), that is, farmers might be trapped in a downward spiral of reduced fallowing and declining crop productivity (de Rouw and Rajot 2004). On the other hand, outmigration of household members (primarily teenagers and young adults) might be offsetting rural population growth, which allows farmers to pursue fallowing. In general, the fallow practices adopted in rain-fed cultivation are comparable across most parts of the Sahel, where croplands are fragmented into small sized fields (Turner and Moumouni 2018).

170

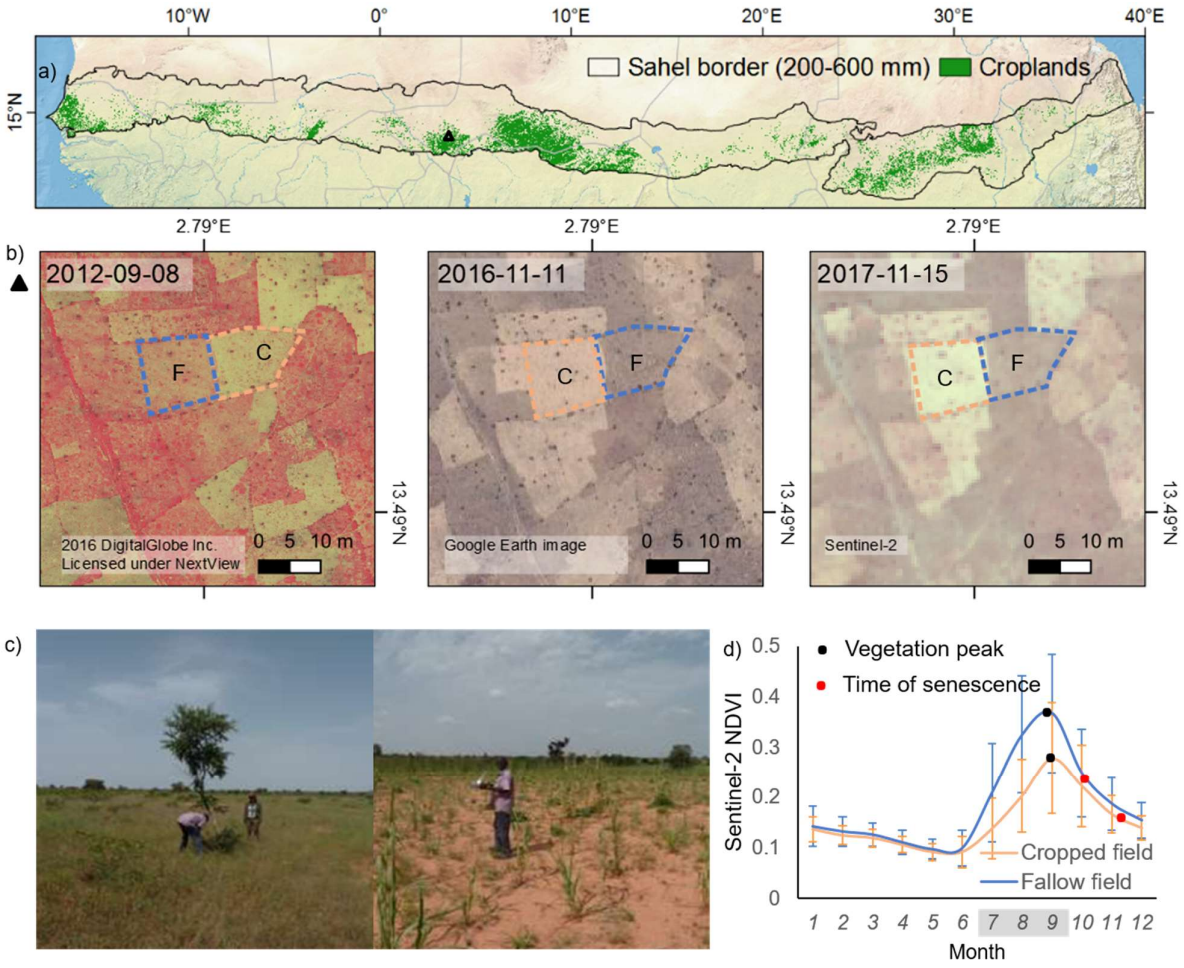

171

172 Figure 1. a) The study area of Sahelian croplands from the Copernicus Dynamic Land Cover map of
173 2015 (CGLS-LC100) with irrigated cropland excluded (see section 2.2.3). The CGLS-LC100
174 cropland map does not separate fallow fields from cropland. The borders of Sahel were derived
175 from CHIRPS rainfall data (Funk et al., 2015) with 200 and 600 mm isohyets defining the northern
176 and southern extent, respectively. The triangle mark the region covering b) and c) in southern
177 Niger. b) Satellite images showing Sahelian cropland composed of a mixture of cropped fields (C:
178 outlined by an orange dashed line) and fallowed fields (F: outlined by a blue dashed line) from three
179 different years (2012; growing season, 2016 and 2017; end of growing season). Left: WorldView-2
180 (2m resolution) showing fallow fields in red color (false color composite with the near-infrared
181 band shown as red color) indicating higher vegetation coverage, while cropped fields are shown in
182 bright white/yellowish color due to the soil cover. Right: same but from Sentinel-2 at 10m
183 resolution (RGB = bands 8, 4, 3). Middle: Google Earth true-color composite. c) Two field photos
184 (by Hiernaux, P. in Sept. 2016) showing denser (and greener) vegetation covering fallow fields
185 (left) as compared to cropped fields (right), covered by a substantial fraction of bare soil. d)

Sentinel-2 NDVI profiles of cropped and fallow fields based on average values of sample pixels identified across the study area (see Section 2.3.1) and 95% confidence intervals (Fig. S1 shows the NDVI profiles of cropped and fallow fields in two rainfall regimes (arid and semi-arid)).

2.2 Data

2.2.1 Sentinel-2 imagery in Google Earth Engine

We used the GEE archived collection of Top-of-Atmospheric corrected Sentinel-2 (MSI Level-1C) 2017-2018, which includes both Sentinel-2A and 2B, achieving a repeat cycle of five days. NDVI was calculated for each image in GEE based on the 10 m visible and near-infrared (VNIR) spectral bands. Clouds were masked using the QA60 band of the S2 L1C product providing cloud state information. No atmospheric correction was applied on the S2 L1C images, as no server-side function (optimized for Earth engine data cube processing) is currently available in GEE and the S2 L2A Surface Reflectance product (TOA corrected to Surface Reflectance using sen2cor: https://step.esa.int/main/third-party-plugins-2/sen2cor/) is only available in GEE for the African continent with a starting year of 2019.

2.2.2 *MODIS NDVI*

Given the documented superiority of the MODIS data for mapping plant phenological events due to the daily temporal resolution (Estel et al., 2015; Massey et al., 2017), we used the MODIS NDVI seasonality to define the optimal acquisition time window of Sentinel-2 imagery for the separation of active cropped fields and fallow fields (section 2.3.1). The MODIS 8-day composite land surface reflectance product (MOD09Q1, collection 6, spatial resolution 250 m) was used to calculate the NDVI during 2017 (Vermote et al., 2002). MOD09Q1 provides adequate observations for extracting Sahelian vegetation phenology, as the product minimizes the impacts from viewing geometry, cloud cover and aerosol loading and retains at the same time a suitable temporal resolution (Fensholt et al., 2015).

2.2.3 Land cover data

The land cover map of CGLS-LC100 produced by Copernicus Global Land Service (Copernicus Global Land Service, 2019) is freely available at a global scale and at 100 m spatial resolution (https://land.copernicus.eu/global/products/lc). In addition to CGLS-LC100, five cropland products (covering the extent of West Africa, Africa and globally) were selected to assess their respective fallow extents. We included the ESA land cover map (ESA CCI 300 m produced at a global scale:http://maps.elie.ucl.ac.be/CCI/viewer/index.php), the GlobeLand30 (Chen et al., 2015; global, 30 m) and GFSAD30 (Xiong et al., 2017; Africa, 30 m: https://croplands.org/downloadLPDAAC) land cover products, both of which are reported to have a high accuracy (Samasse et al., 2018). Finally, the Sudano-Sahelian cropland map (Lambert et al., 2016) and the West Africa land cover map (Tappan et al., 2016) were included, both specifically created for West Africa. Despite a coarser resolution of 2 km, the West Africa land cover map is considered a valuable land cover

product for this study, as the cropland extent is assessed from an extensive process based on visual interpretation of imagery and expert knowledge.

The cropland class of the above-mentioned maps include irrigated cropland (Fig. S1), which was masked out using the ESA CCI 300 m map of 2015.

Table 1. Characteristics of the applied land cover products.

Product	*Class*	*Data*	*Resolution*	*Coverage*	*Year*
CGLS-LC100	Cropland	PROBA-V	100 m	Africa	2015
ESA CCI 300 m	Rainfed cropland	PROBA-V	300 m	Global	2015
GlobeLand 30	Cultivated land	Landsat	30 m	Global	2010
GFSAD30	Cropland	Landsat	30 m	Global	2015
Lambert et al.2016	Cropland	PROBA-V	100 m	West Africa	2015
Tappan et al.2016	Cropland	Landsat	2 km	West Africa	2013

2.3 Mapping cropped and fallow fields

The analysis consists of the mapping of cropped and fallow fields and the assessment of the extent of fallow areas within croplands as classified by contemporary land cover products (Fig. 2). The mapping was done in two steps: (a) A reference dataset (section 2.3.1) was generated in a hierarchical manner by first selecting optimal Sentinel-2 imagery from the dry down period of the growing season (period locally defined by MODIS seasonal metrics for each 0.15° grids) and then extracting reference data information in a two-stage process. (b) Cropped and fallow fields were separated using the generated reference data and annual NDVI time series of Sentinel-2 (section 2.3.2) (c) The extent of fallow fields was assessed for selected contemporary cropland products. The cropped/fallow field ratio was analyzed in relation to rainfall and woody cover (section 2.3.3).

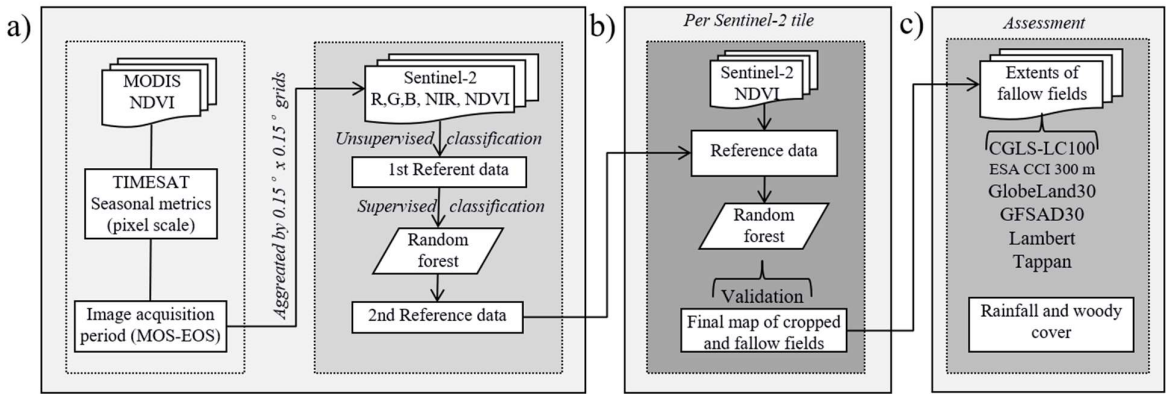

Figure 2. Flowchart of the methods applied: a) Generation of reference data for actively cropped and fallow fields within each 0.15° grid across the study area. b) Mapping of cropped and fallow fields using the Sentinel-2 NDVI time series based on enhanced training dataset. Results were evaluated per Sentinel-2 tile (100x100 km^2). c) Assessment of the extent of fallow areas within croplands as classified by contemporary land cover products, and analysis of the relationship between rainfall, woody cover and mapped fields.

2.3.1 Generation of reference data

The generation of reference data was done in three steps: (1) selection of Sentinel-2 images through seasonal metrics within grid cells, (2) creation of a first reference dataset through unsupervised classification, (3) refinement of this first reference dataset into an enhanced (second) version of the reference dataset through a supervised classification.

(1) We derived seasonal metrics from MODIS NDVI for the year 2017 to define the period representing the maximum spectral difference between cropped and fallow fields, which is located around dry-down period of the growing season. This period was used to define the start and end time of the relevant Sentinel-2 imagery acquisition period. The seasonal metrics were extracted from the MODIS 8-day NDVI composites using the TIMESAT software (Jönsson, & Eklundh, 2004): a tool for parameterization of vegetation phenology from satellite time series data. In TIMESAT, we set the window size to 4, the seasonal parameter to 0.5 to fit one season per year, the number of iterations for upper envelope adaptation to 2, and the strength of the envelope adaptation to 2. The time of the mid of season (MOS) was computed as the average time between the green-up phase (80 % of the amplitude before the maximum), and the dry-down phase (80 % after maximum) (Eklundh and Jönsson, 2017). The end of season (EOS) was set to 50% after the maximum (Zhang et al., 2018).

The study area was segmented into 0.15° x 0.15° grids in which the MOS and EOS dates were averaged from the MODIS pixels within each grid. The size of the grid cells was selected by trial and error and is a compromise being big enough to include both crop/fallow classes, but do not exceed the size beyond which local landscape characteristics disappear. The Sentinel-2 image acquisition was then guided by the MOS and EOS dates determined for each grid cell individually. For each grid, Sentinel-2 images with a cloud cover larger than 10% were excluded and to further reduce the impacts from clouds and burned areas, compositing of the remaining Sentinel-2 image series (VNIR and NDVI between MOS and EOS) was produced by taking the median value for the subsequent analysis.

(2) we created a first reference dataset based on the fact that cropped fields generally have a lower NDVI than fallow fields (Tong et al., 2017). We randomly selected one million pixels (a resolution of 10m x 10m) within the study area. Out of these one million pixels, we automatically classified the pixels within each 0.15° x 0.15° grid as follows: A) each pixel was classified into two classes as either cropped or fallow based on Sentinel-2 visible bands, NIR band and NDVI using WEKA

(Waikato Environment for Knowledge Analysis) unsupervised classification (Tony & Eibe, 2016). B) Given that an unsupervised classification normally produces outputs with a rather low accuracy in cases of spectral similarities, we only used the pixels with the lowest (in respect to NDVI values) 25% of the cropped fields class and the highest 25% of the fallow fields class as the reference dataset in the first stage.

(3) We created an enhanced second reference dataset generated from the first reference dataset produced. This step was deemed necessary as the generated reference dataset tended to cluster in large-size fields, leading to an unbalanced representation of the fallow and cropped fields within each grid. To overcome the issue of spatial clustering, small field patches (usually evenly scattered across the landscape) were targeted for selecting an enhanced reference dataset in this second stage. This was achieved by using the first stage reference dataset from the WEKA unsupervised classification as input for a Random Forest (RF) classifier, which was applied for each 0.15° grid. The Random Forest (Breiman 2001) is a non-parametric machine learning classifier widely used for image classification due to its simple parameterization and high classification accuracy (Pelletier et al., 2016). For each grid cell, the values of Sentinel-2 spectral bands and NDVI of the reference pixels were used as predictor variables to predict the crop and fallow classes. RF randomly split the inputs into user-defined number of trees (=500) as larger values are known to have little influence on the overall classification accuracy (Breiman and Cutler 2007). RF assign the class labels based on the majority vote among all bootstrapped classification trees. We then extracted small cropped and fallow field patches over the entire study area from the RF classification results by applying a spatial morphological analysis, for which only connected areas within a range of 10-20 Sentinel-2 pixels targeting individual fields of one hectare. The enhanced reference dataset was a stratified random sample of pixels from those small cropped and fallow field patches. For validation of the enhanced reference data, we generated 200 pixels (100 within cropped and 100 within fallow fields) within the CGLS-LC100 cropland extent of the Sahel and visually evaluated the accuracy based on the Sentinel-2 false-color image composites. These pixels were used to create Figure 1d (only a total number of 183 true positive pixels were used (93 pixels of cropped fields and 90 pixels of fallow fields) (see section 3.2)).

2.3.2 Random Forest classification using an enhanced reference dataset

The full-year Sentinel-2 NDVI time series, representing one year of crop phenology, was used as predictor variables for the final crop/fallow land classification. The Random Forest classifier was parameterized the same way as outlined in section 2.3.1 and was applied on all individual Sentinel-2 tiles with cloud cover less than 5%. For each Sentinel-2 tile, each decision tree grows on an independent bootstrap sample from the training data. A total number of 2000 stratified random sample pixels were generated within the extent of small-size field patches of each tile (1000 within cropped and 1000 within fallow fields). A total of 80% of the sample data was used for training and 20% for validation.

2.3.3 Spatial distribution of cropped and fallow fields

We analyzed the associations between the crop-fallow ratio and a) rainfall and b) woody cover (Fig. S6). Average annual rainfall was calculated using the CHIRPS data (Funk et al., 2015) from 1981 to 2018. The ratio between cropped and fallow fields was calculated for each 50 mm rainfall interval. The woody cover, predicted as 0-100% at 100 m resolution, was used to characterize differences in the woody cover in cropped and fallow fields (Brandt et al., 2018). The mean woody cover was calculated for cropped and fallow fields, respectively, and for the arid (200-300 mm rainfall) and semi-arid (300-600 mm rainfall) zones, based on woody cover data covering the western Sahel for a nominal period of 2014-2016. Finally, we examined the spatial distribution of cropped and fallow fields among the six selected contemporary cropland products.

3. Results

3.1 Phenology-based selection of Sentinel-2 imagery

The MOS and EOS (defining the start and end date of Sentinel-2 imagery acquisitions) varied across the Sahel (Fig. 3), with a majority of the croplands characterized by MOS in August. A later MOS (September) is observed in the westernmost Sahel (Senegal), while an early MOS (July) appears in smaller areas in the eastern Sahel. The EOS predominantly occurs in October for the northern Sahel and in November for the southern Sahel, making the period between vegetation peak and end of the growing season (time between MOS and EOS) relatively shorter in northern Sahel than southeastern Sahel. The MOS showed generally small variations (as indicated by the standard deviations (Fig S3)) across the Sahel (0-10 days), while a stronger variation (10-20 days) was observed in the EOS.

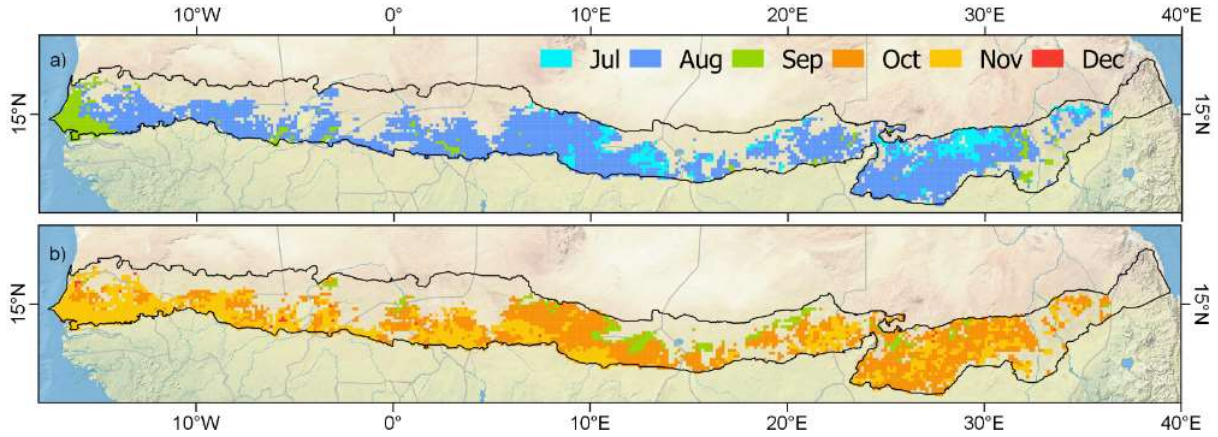

Figure 3. The time window of Sentinel-2 image acquisition defined by the period between (a) MOS and (b) EOS (averaged per 0.15° grid) within the study area of Sahelian croplands (Fig. 1a). The exact per-pixel Day-Of-Year and the standard deviation are shown in Fig. S3 and S4.

The availability of cloud-free Sentinel-2 imagery ranged from 3 to 40 images during the acquisition period (from MOS to EOS) for each 0.15° grid (Fig. 4a). The average image availability per grid was three images, which was sufficient to create high-quality median images for the entire study area (Fig. 4 b, c, d). The spectral difference between cropped and fallow fields are captured across space by the median image from the acquisition period. However, the strength of this difference (expressed by vegetation greenness shown as red color in Fig. 4b-d) varies with rainfall abundance from southern Sahel (Fig. 4b) to central/northern Sahel (Fig. 4c and 4d) and farming techniques (such as manure or fertilizer application).

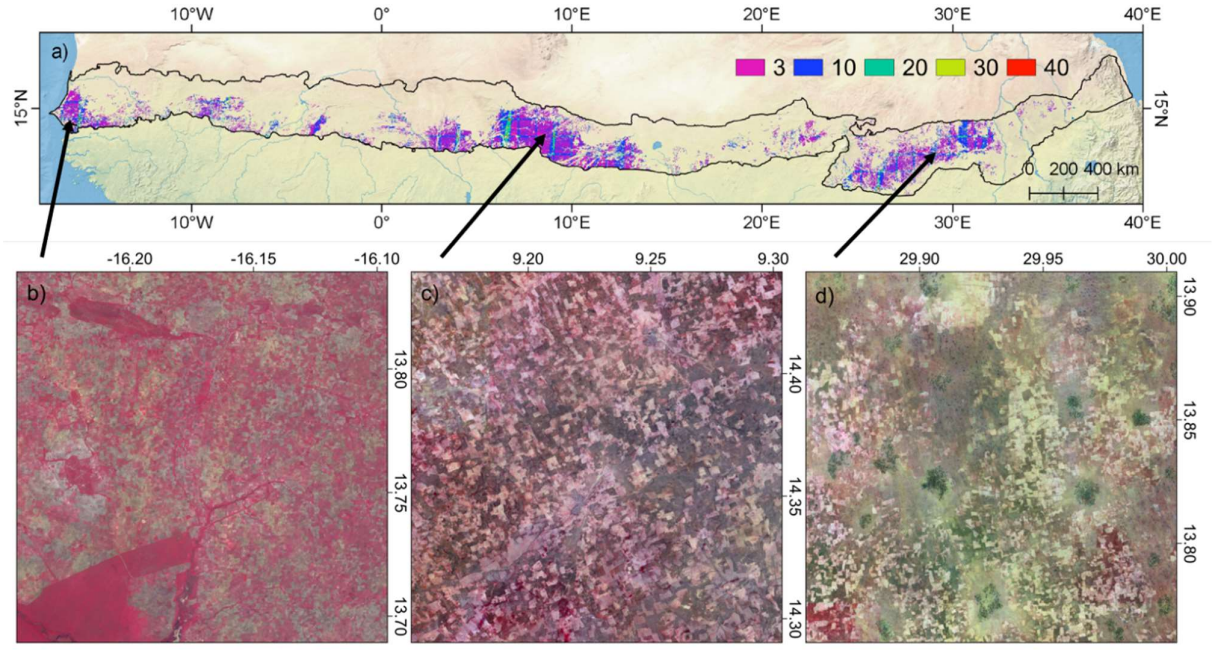

Figure 4. a) Number of cloud-free Sentinel-2 images for 2017 within the pheno-defined period for each grid. b-d) are three example median false-color composite images (RGB = bands 8, 4, 3) during the pheno-defined period in Senegal (MOS: September, EOS: November), Niger (MOS: August, EOS: October) and Sudan (MOS: July, EOS: September), respectively.

3.2 Generating reference data

The reference data from the unsupervised classification provided ~400 000 sample pixels for the entire study area. Although the initial generation of reference dataset of the two classes (cropped and fallow fields) revealed a reasonable performance, the spatial distribution of sample pixels was not homogeneous within the 0.15° grids (Fig. 5a). The generation of enhanced reference dataset from the RF classification (Fig. 5 b-e) shows the spatial distribution of the final enhanced reference dataset, which are small-sized cropped and fallow field patches (see section 2.3.1). The validation based on Sentinel-2 false-color composites yielded an overall accuracy of 84% (153/183) with a

crop and fallow user's accuracy of 73% and 91% and a producer's accuracy of 90% and 79%, respectively. We found 8.5% (17/200) of the validation sample pixels to be located in bare land (7/17) or natural vegetation (10/17) due to misclassification in the CGLS-LC100 cropland mask.

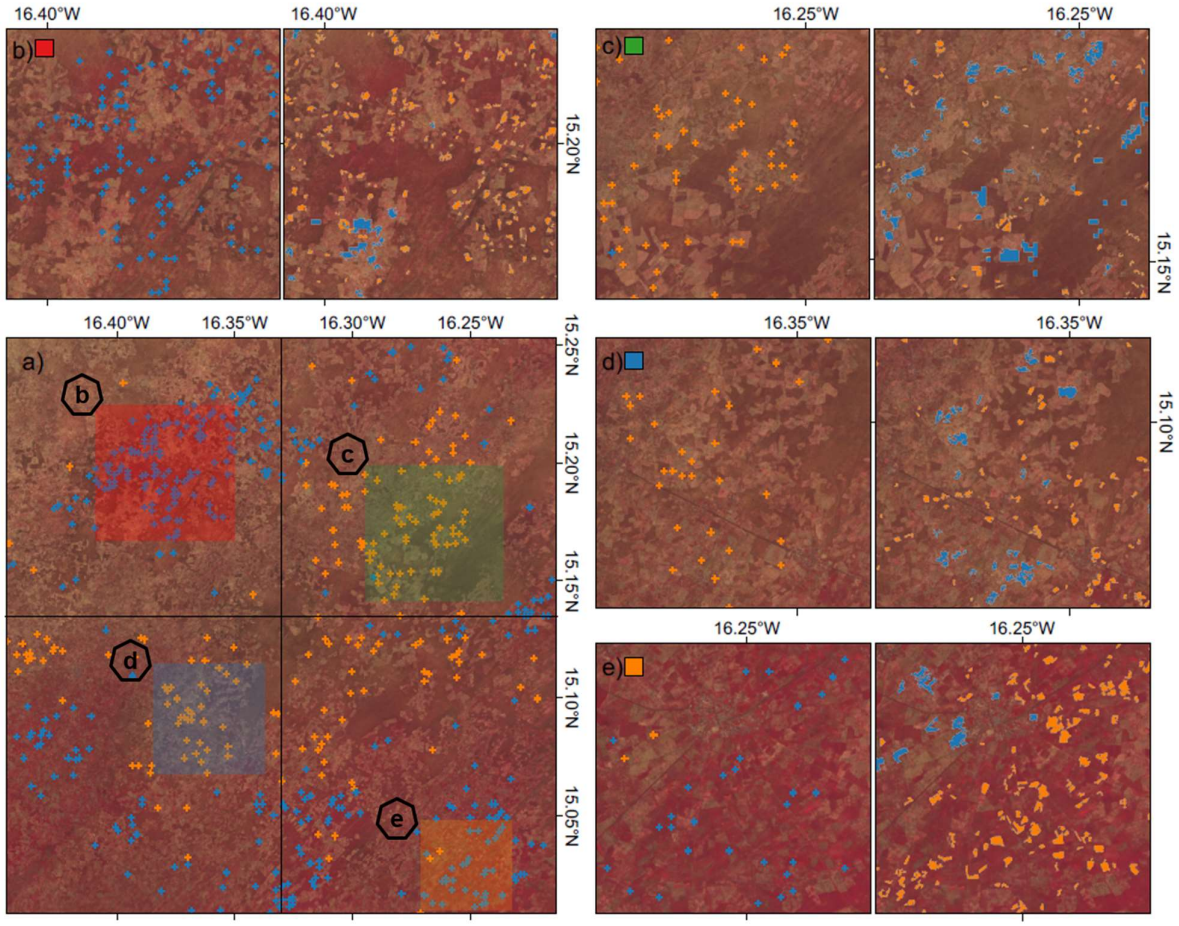

Figure 5. a) Sentinel-2 false-color composites (RGB = bands 8, 4, 3) of four 0.15° grids. The crosses show reference data from the unsupervised classification (blue= fallow; orange= cropped). The sub figures b-e) are zoom-ins (corresponding to the colored blocks in a)). The left-hand side zoomed images show the reference from the unsupervised classification (as in a), whereas the right-hand side shows the final enhanced reference dataset. The final reference dataset generated covering the same area is shown in Fig. S5.

3.3 Mapping cropped and fallow fields

The enhanced reference dataset was used for the final RF classification resulting in a map showing cropped and fallow fields ubiquitously distributed over the Sahel for the year 2017 at 10 m resolution (Fig. 6). The overall accuracy of cropped and fallow field map ranged from 73 % to 94 %

amongst 223 tiles (Fig S7 and Table S1) with an average accuracy of 88%. Larger trees in the cropped fields with a crown size exceeding 10x10 m were typically mapped as fallow pixels but were excluded in our assessment by using a filter identifying fallow fields which were smaller than three connected pixels (considering both trees and tree shadows). The identified trees (15,963 km^2) were added into the class of cropped fields instead as they belong to the extent of active cropland. Both smaller and larger fields were successfully classified (Fig. 6b-i: darker red areas are fallow fields and the bright areas represent cropped fields).

Local cases of error also occur where croplands have been missed in the CGLS-LC100 classification (Fig. 6b, d, g) and mapped as non-cropland (in grey color) which can be identified by visualizing the patterns of the cropped field from false color composites (bright white/yellow color, Fig. 1b). Occasionally, degraded land (shown as the brighter light green color of Fig. 6f) and natural vegetation (shown as darker red color on the top-right corner of Fig. 6e) have been included in the cropland class, leading to misclassified cropped and fallow fields. Some patches of fallow fields around villages have been mapped as cropped fields (Fig. 6i) since the seasonal NDVI profile of these fields is similar to that of cropped fields, likely due to poor soil fertility or/and intense grazing. Furthermore, cropped fields surrounding villages are often manured (see areas around the village in the central part of Fig. 6b and the lower-right corner of Fig. 6d), leading to increased soil fertility and thus higher greenness, which can result in misclassifications of these fields as fallow.

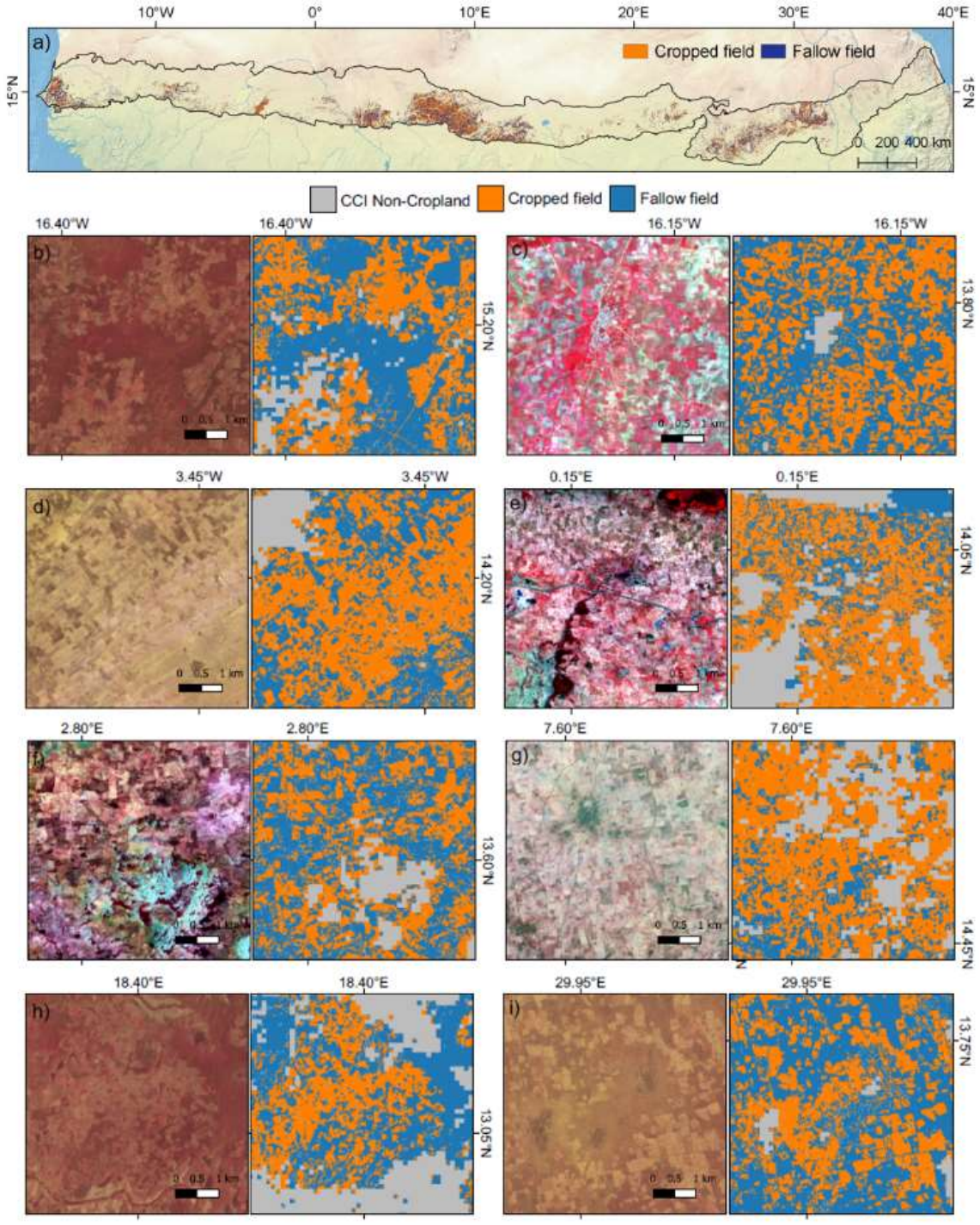

Figure 6. a) Classification of cropped and fallow fields at 10 m for the Sahel. (b) to (i) show zoom-ins with the false-color composite (RGB = bands 8, 4, 3) Sentinel-2 image on the left-hand side and the classification results on the right-hand side. b) Example from northern Senegal, c) from southern Senegal, d) central Mali, e) northern Burkina Faso, f) western Niger, g) eastern Niger, h)

Chad, i) Sudan. The mapping result can be visualized via a web viewer (https://buwuyou.users.earthengine.app/view/fallowinsahel).

3.4 The spatial distribution of cropped and fallow fields

Within the extent of CGLS-LC100 cropland areas, the ratio of cropped to fallow areas decreases along the rainfall gradient and stabilizes at the level of 0.5-0.6 coinciding with the transition from the arid to the semi-arid zone (around 300 mm/year) (Fig. 7a). Woody cover is on average 7.6 and 10.6% for cropped and fallow fields, respectively. However, in the arid zone woody cover is higher in the cropped fields as compared to fallow fields whereas in the semi-arid zone a reversed pattern is seen (Fig. 7b).

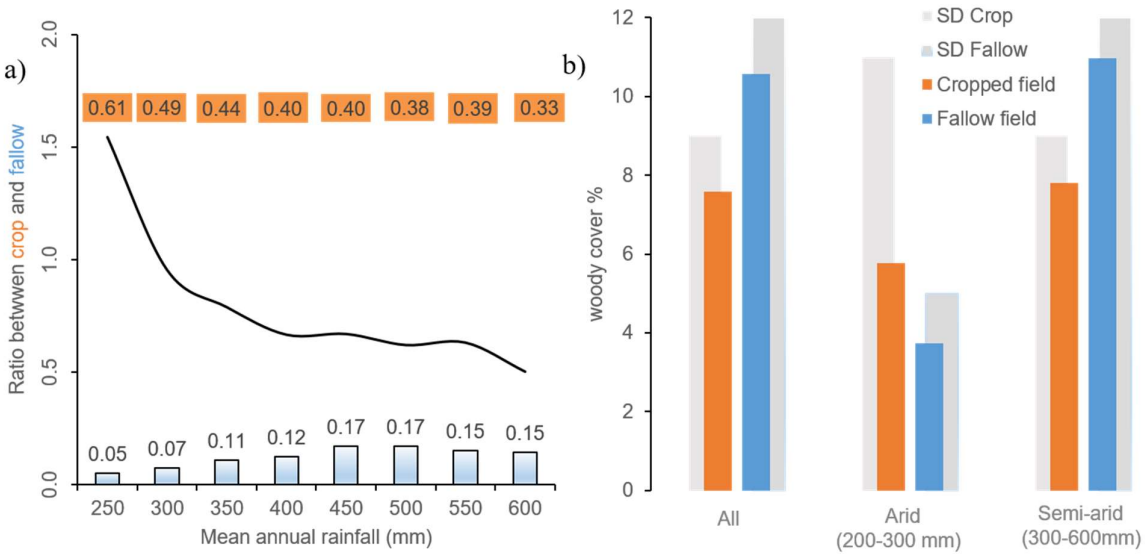

Figure 7. a) The dark line shows the ratio of cropped to fallow area along the rainfall gradient (50 mm steps) from 200 to 600 mm, while the bar plots (blue color) show the fraction of cropland pixels in Sahel for each rainfall interval (total number of Sentinel-2 pixels = 65 918 900). The numbers in orange text boxes show the fraction of cropped field within croplands along the rainfall gradient. b) The average woody cover (%) is shown for cropped and fallow fields, respectively, in the arid and semi-arid zone.

The areal extent of detected fallow fields for six state-of-the-art land cover products shows that there were more fallow fields than cropped fields within the cropland class of all examined land cover products, with fallow land ranging from 57% to 63% (Table 2). Although the cropland products differ in methodology, spatial pattern and cropland extension, the fallow/cropland percentage ratio is observed to be relatively stable.

Table. 2 Sahelian cropland and fallow extent (km^2) in selected cropland products. Cropland/fallow extent was assessed for the area between the 200 and 600 mm isohyets (derived from CHIRPS rainfall data (Funk et al., 2015)), defining the northern and southern extent of Sahel, respectively.

Product (km^2)	*CGLS-LC100*	*ESA CCI 300 m*	*Globland30*	*GFSAD30*	*Lambert et al., 2016**	*Tappan et al., 2016**
Cropland area	403 617	793 332	264 321	340 643	258 985	266 510
Fallow area	255 572	460 882	163 448	209 108	156 966	152 248
Cropped area	148 045	332 450	100 873	131 535	102 109	114 262
Cropped/Fallow	37/63%	42/58%	38/62%	39/61%	39/61%	43/57%

* Products only cover the western and central Sahel

4. Discussion

4.1 Uncertainties in fallow fields mapping at sub-continental scale

Our method relies on a high accuracy cropland map as a starting point. Although cropland mapping accuracy has improved recently, none of the existing cropland maps consistently reach a 75% accuracy threshold among Sahelian countries (Samasse et al., 2018), hence errors of commission and omission are present in the cropland masks, which propagates into the fallow mapping. Some of the examples shown in Fig. 6 (particularly b from Senegal) show larger contiguous 'fallow' areas around more intensively cultivated areas. These examples can be interpreted as cases causing an overestimation of the fraction of cropland being fallowed. The CGLS-LC100 "cropland" may include some misclassified rangelands and eroded bare lands which will then be an error source propagating to the extraction of cropped and fallow fields. Besides, there are also cases where cropped fields are not included in the lands mapped as "cropland" (Fig. 6d). The manured fields and fields with denser tree cover (agroforestry parklands) can be misclassified as fallow fields while heavily grazed fallow fields can be miss-classified as cropped fields. Such effects will inevitably also be present in the process of reference data generation. Finally, though using a different land cover product (MODIS land cover), the study of Leroux et al. (2014) suggested that the user accuracy of the cropland class varies with different rainfall regimes and the associated cropping systems (e.g. agropastoral millet/sorghum, cereal-root crop mixed and irrigated farming systems). Therefore, the statistical analysis between the ratio of cropped to fallow area and rainfall gradients and woody cover should be interpreted with caution.

The mapping methodologies described in sections 2.3.1 and 2.3.2 are based on slightly different solutions coping with the challenges of either generating reference data using unsupervised classification (step 'a' in Fig. 2) or predicting cropped and fallow fields with random forest (step 'b'

in Fig. 2). For the unsupervised classification, we used the median value of the Sentinel-2 spectral bands between the MOS and EOS to make use of spectral information and reduce the high dimensional feature space. Machine learning algorithms like random forest have shown to work well with seasonal time series (Brandt et al., 2018) and can deal with a high-dimensional feature space, so we opted for the use of the full NDVI time series for the random forest classification. As for the generation of reference data, the suggested method provides a framework for extracting reference data from small-size field patches without manual digitizing work. No additional steps were implemented to avoid including >2 pixels from the same patch when generating the 2000 stratified random sample pixels for validation, due to the massive computational workload in vectorizing small-size patches across Sahel. However, given the large number of patches (SFig.5 shown hundreds of patches within 30 X 30 km^2) this is not expected to have implications for the results.

Finally, some standard image pre-processing procedures are currently not implemented in GEE, such as atmospheric correction, which is important for large-scale mapping when using multiple images and particular when building one universal model for mapping the entire study area. This is however not the case here, as we produced separate random forest models for the geographical coverages matching the extent of each Sentinel-2 tile. Still, we used NDVI that will be affected by atmospheric conditions, yet the impact from such perturbations will influence equally on the NDVI temporal signatures of crop and fallow fields. How big such influence is, depends on the magnitude of the difference between NDVI of cropped/fallow fields.

4.2 Fallowing in the Sahel

Our study achieves an overall accuracy of 88% and provides a benchmark map of fallow fields across the Sahel which can facilitate an improved understanding of how crop-fallow rotation cycles are linked to agricultural management practices, pressure on land, soil fertility and food security. A surprising finding of this study is the high percentage of fallow in the croplands of the Sahel. This suggests that regeneration of soil fertility through fallowing plays a greater role – relative to replenishment of plant nutrients by recycling livestock manure or importing mineral fertilizers – than previously expected (Schlecht et al., 2004). However, that there are inherent challenges associated with separating fallow from grazing areas within Sahelian croplands (as introduced in section 4.1). Most of the areas classified as fallow are used for grazing, both by livestock owned by local farmers and herds owned by pastoralists from outside, passing through, and part of the manure from these herds is collected and transported to cropped fields. Hence, we cannot exclude the possibility of misclassification of rangelands as fallow, caused by the cropland mask (used for delineation of the area of analysis) being too inclusive. Indeed, a multi-year assessment of grass fallowing is expected to harness the fallow field mapping in this aspect, since separation of fallow from grazing areas independently from using a cropland mask, would only be feasible from analyzing states of multiple years. Finally, as noted above, intensive manuring of fields close to villages may give rise to misclassifications, as may intensive grazing close to villages. Whether some fallows, located within otherwise cultivated areas, are actually semi-permanent grazing reserves probably cannot be determined without the use of longer time-series of Sentinel-2 data.

The results show that a considerable extent of what is often mapped as cropland did actually not produce crop yields in 2017, which needs to be considered when food production is estimated based on cropland products. The fact that fallow fields dominate over cropped fields contradicts common narratives that population pressure and increased demand for food have caused a Sahel-wide extinction of fallow practices leading to unsustainable land management systems (Pieri 1989; Lüdeke et al., 2004). However, fallowing and cropping of fields vary over time and space, and monitoring of the dynamics (crop-fallow rotation cycle and trends of changes between cropped and fallow fields) is essential to fully understand land management in the Sahel. Not only a decreasing spatial extent of fallow areas but also a shortening of the fallow cycle (for example in western Niger un-manured sandy soils need at least three years of fallow to recover its fertility after five years of millet cropping (Hiernaux and Turner, 2002)) is a sign of eroding soil fertility which can lead to poor crop yield and ultimately to food shortages. Future repeated mapping of fallow/cropped field dynamics at the Sahelian scale from the Sentinel-2 constellation may thus be used as an indicator to identify and predict food shortages and emerging land degradation.

The analysis of the relationship between the fraction of agricultural land under fallow and annual rainfall (Fig. 7a) shows an increasing fraction of fallow with increasing rainfall. This is in accordance with expectations: Fallows serve as a means of soil regeneration after cropping, and the importance of soil nutrient limitations on crop yields is expected to increase with rainfall in the Sahel (Penning de Vries and Djiteye, 1982). Also, nutrients from manure are, all other factors even, more readily available in the northern part of Sahel, dominated by pastoralism. As expected, woody cover (including both trees and shrubs) in fallow fields was generally higher than in cropped fields (Fig. 7b). When a field is left for fallow, bushes and shrubs are not being removed and are able to spread. These shrubs help regenerating the soil fertility, and serve as a source of wood used as fuelwood, for construction and medical purposes by the local population. Once a field is changed from fallow to cropland, shrubs and bushes are typically coppiced and only trees having reached a certain height are kept. It should be noted that the result is potentially sensitive to the above-mentioned challenges of misclassification of rangelands as fallow (a problem inherited in the cropland masks used). Since the woody vegetation in fallow fields consists of few individual trees (as in cropped fields) and a high abundance of bushes turning into shrubs as the fallow gets older, fallow differs from rangeland woody populations often more gradually distributed in size and patchier in space. A better separation of fallow from grazing land may be achieved by assessing the height distribution of the woody vegetation.

4.3 Options for future improvements of fallow mapping

In this study, Sentinel-2 has proved to be useful in separating individual fields. Since 2013, Landsat 8 has collected 30 m images with a global coverage every 16 days. The integration of Landsat and Sentinel-2 (Claverie et al., 2018; Yan et al., 2016) would significantly increase the temporal resolution of annual time series, but with known effects of spatial misalignment between images (Carrasco et al., 2019). However, the increased temporal resolution of a merged dataset has already been used to separate crop types (Griffiths et al., 2019), which could be the next step in better characterizing Sahelian land use practices. The fallow mapping presented here is confined by using

a common ‘cropland’ land cover map. Based upon time series of high resolution satellite data agricultural land can instead be mapped into different classes characterizing management practices of cropped fields: permanent, shifting with short, medium, long duration fallow. Ultimately, continuous mapping of the per-pixel crop/fallow cycle will allow for studies targeting land use intensification/extensification of areas of smallholder agriculture.

A rapid increase in the number of large-scale and high resolution multi-temporal remote sensing applications is seen in recent years, based on free cloud platforms, such as GEE, to process thousands to millions of 10-30 m image tiles (Pekel et al., 2016; Dong et al., 2016; Xiong et al., 2017; Huang et al., 2017). GEE is not only a platform to store large quantities and varieties of satellite datasets, it also provides an increasing number of image processing algorithms including machine learning classification algorithms (e.g. support vector machine and RF). The increasing availability of free and open-source cloud platforms (such as the so-called Earth Observation Data Cube; https://www.opendatacube.org/) will provide analysis ready data and advanced tools to advance environmental monitoring using remotely sensed Earth Observations (EO) data (Giuliani et al., 2017). In recent years, deep learning technology has been increasingly available for image recognition and object detections. For crop-wise classification, deep learning models do not require pre-determined curve functions or mathematical assumptions for crop seasonality in specific areas (Zhong et al., 2019). However, the preparation of training sets is still required for such deep learning models. Considering the challenging field objects with various shapes, models need to be tested for the separation of cropped and fallow fields if a suitable architecture is to outperform traditional machine learning algorithms.

5. Conclusion

Enabled by new high-quality Sentinel-2A and -2B images and GEE cloud computing, this study presents a totally covering, yet very detailed, account of the extent of fallow lands within the Sahel agricultural lands mapped as “cropland” in global and regional products. We found that fallow fields, which are often neglected in agricultural land assessments, occupied 57-63% of Sahelian agricultural lands in 2017 (calculated among six different state-of-the-art remote sensing cropland products). The accuracy of the cropland products, serving as a point of departure for the numbers reported here, should however be kept in mind when interpreting the fallow extent, as misclassifications of natural vegetation in the cropland class will propagate to the estimated extent of fallow fields. From the combined use of satellite datasets of both high and low spatial resolution and varying temporal resolution, our designed two-step automated reference data generation workflow is spatially representative for the landscape studied and highly reproducible. The proposed method is therefore applicable for continuous fallow mapping based on multiple years of data to understand the dynamics of crop-fallow rotation cycles in the Sahel and similar agricultural systems. As such, the EO-based mapping (with publicly available, free data) of cropped and fallow fields opens new avenues for agricultural monitoring, e.g. for purposes of land use intensification/extensification, ‘famine early warning’ and agricultural statistics. Finally, our

findings advance current understandings of agricultural systems in the region as they demonstrate how fallow plays a greater role than previously assumed as fallow land occupy more than half of the area included in the 'cropland masks' available.

Acknowledgements

The primary funding of this research is from the China Scholarship Council (CSC, number 201407650011), the AXA post-doctoral fellowship , and the Danish Council for Independent Research (DFF) Grant ID: DFF – 6111-00258. We would like to thank the three anonymous reviewers for their thorough and constructive comments.

589
590 References

591 Achard F., P. Hiernaux & M. Banoin, 2001. Les jachères fourragères naturrelle et améliorée en Afrique de
592 l'Ouest. In Ch. Floret & R. Pontanier (eds) La jachère en Afrique tropicale. De la jachère naturelle à la
593 jachère améliorée. Le point des connaissances. John Libbey Eurotext, Paris: 201-240

594 Begue, A., Vintrou, E., Saad, A., Hiernaux, P., 2014. Differences between cropland and rangeland MODIS
595 phenology (start-of-season) in Mali. Int. J. Appl. Earth Obs. Geoinf. 31, 167–170.
596 https://doi.org/10.1016/j.jag.2014.03.024

597 Bégué, A., Arvor, D., Bellon, B., Betbeder, J., de Abelleyra, D., Ferraz, R.P.D., Lebourgeois, V., Lelong, C.,
598 Simões, M., Verón, S.R., 2018. Remote sensing and cropping practices: A review. Remote Sens. 10, 1–32.
599 https://doi.org/10.3390/rs10010099

600 Brandt, M., Rasmussen, K., Hiernaux, P., Herrmann, S., Tucker, C.J., Tong, X., Tian, F., Mertz, O., Kergoat,
601 L., Mbow, C., David, J.L., Melocik, K.A., Dendoncker, M., Vincke, C., Fensholt, R., 2018. Reduction of tree
602 cover in West African woodlands and promotion in semi-arid farmlands. Nat. Geosci. 11, 328–333.
603 https://doi.org/10.1038/s41561-018-0092-x

604 Breiman, Leo. 2001. "Random Forests." Machine Learning 45 (1): 5–32.
605 https://doi.org/10.1023/A:1010933404324.

606 Breiman, L., and Cutler, A. 2007. "Random forests - Classification description." RandomForests,
607 https://www.stat.berkeley.edu/~breiman/RandomForests/cc_home.htm (accessed 7 Feburary 2019)

608 Carrasco, L., O'Neil, A.W., Daniel Morton, R., Rowland, C.S., 2019. Evaluating combinations of temporally
609 aggregated Sentinel-1, Sentinel-2 and Landsat 8 for land cover mapping with Google Earth Engine. Remote
610 Sens. 11. https://doi.org/10.3390/rs11030288

611 Chen, J., Chen, J., Liao, A., Cao, X., Chen, L., Chen, X., He, C., Han, G., Peng, S., Lu, M., Zhang, W., Tong,
612 X., Mills, J., 2015. Global land cover mapping at 30 m resolution: A POK-based operational approach.
613 ISPRS J. Photogramm. Remote Sens. 103, 7–27. https://doi.org/10.1016/J.ISPRSJPRS.2014.09.002

614 Claverie, M., Ju, J., Masek, J.G., Dungan, J.L., Vermote, E.F., Roger, J.-C., Skakun, S. V., Justice, C., 2018.
615 The Harmonized Landsat and Sentinel-2 surface reflectance data set. Remote Sens. Environ. 219, 145–161.
616 https://doi.org/10.1016/j.rse.2018.09.002

617 Cooper, P.J.M., Dimes, J., Rao, K.P.C., Shapiro, B., Shiferaw, B., Twomlow, S., 2008. Coping better with
618 current climatic variability in the rain-fed farming systems of sub-Saharan Africa: An essential first step in
619 adapting to future climate change? Agric. Ecosyst. Environ. 126, 24–35.
620 https://doi.org/10.1016/J.AGEE.2008.01.007

621 Copernicus Global Land Service, 2019. Copernicus Global Land Service Copernicus global land service-
622 land cover: https://land.copernicus.eu/global/products/lc (accessed on 14 September 2019)

623 Cracknell, M.J., Reading, A.M., 2014. Geological mapping using remote sensing data: A comparison of five
624 machine learning algorithms, their response to variations in the spatial distribution of training data and the
625 use of explicit spatial information. Comput. Geosci. 63, 22–33.
626 https://doi.org/10.1016/J.CAGEO.2013.10.008

De Ridder, N., Breman, H., Van Keulen, H., Stomph, T.J., 2004. Revisiting a "cure against land hunger": Soil fertility management and farming systems dynamics in the West African Sahel. Agric. Syst. 80, 109–131. https://doi.org/10.1016/j.agsy.2003.06.004

De Rouw, A., Rajot, J.L., 2004. Nutrient availability and pearl millet production in Sahelian farming systems based on manuring or fallowing. Agric. Ecosyst. Environ. 104, 249–262. https://doi.org/10.1016/j.agee.2003.12.019

Dong, J., Xiao, X., Menarguez, M.A., Zhang, G., Qin, Y., Thau, D., Biradar, C., Moore, B., 2016. Mapping paddy rice planting area in northeastern Asia with Landsat 8 images, phenology-based algorithm and Google Earth Engine. Remote Sens. Environ. 185, 142–154. https://doi.org/10.1016/j.rse.2016.02.016

Douxchamps, S., Van Wijk, M.T., Silvestri, S., Moussa, A.S., Quiros, C., Ndour, N.Y.B., Buah, S., Somé, L., Herrero, M., Kristjanson, P., Ouedraogo, M., Thornton, P.K., Van Asten, P., Zougmoré, R., Rufino, M.C., 2016. Linking agricultural adaptation strategies, food security and vulnerability: evidence from West Africa. Reg. Environ. Chang. 16, 1305–1317. https://doi.org/10.1007/s10113-015-0838-6

Eklundh, L., Jönsson, P., 2017. TIMESAT 3.3 with seasonal trend decomposition and parallel processing Software Manual. http://web.nateko.lu.se/timesat/docs/TIMESAT33_SoftwareManual.pdf (accessed on 9 October 2019)

Estel, S., Kuemmerle, T., Alcántara, C., Levers, C., Prishchepov, A., Hostert, P., 2015. Mapping farmland abandonment and recultivation across Europe using MODIS NDVI time series. Remote Sens. Environ. 163, 312–325. https://doi.org/10.1016/j.rse.2015.03.028

Fensholt, R., Horion, S., Tagesson, T., Ehammer, A., Grogan, K., Tian, F., Huber, S., Verbesselt, J., Prince, S.D., Tucker, C.J., Rasmussen, K., 2015. Assessment of Vegetation Trends in Drylands from Time Series of Earth Observation Data. pp. 159–182. https://doi.org/10.1007/978-3-319-15967-6_8

Fritz, S., See, L., McCallum, I., You, L., Bun, A., Moltchanova, E., Duerauer, M., Albrecht, F., Schill, C., Perger, C., Havlik, P., Mosnier, A., Thornton, P., Wood-Sichra, U., Herrero, M., Becker-Reshef, I., Justice, C., Hansen, M., Gong, P., Abdel Aziz, S., Cipriani, A., Cumani, R., Cecchi, G., Conchedda, G., Ferreira, S., Gomez, A., Haffani, M., Kayitakire, F., Malanding, J., Mueller, R., Newby, T., Nonguierma, A., Olusegun, A., Ortner, S., Rajak, D.R., Rocha, J., Schepaschenko, D., Schepaschenko, M., Terekhov, A., Tiangwa, A., Vancutsem, C., Vintrou, E., Wenbin, W., van der Velde, M., Dunwoody, A., Kraxner, F., Obersteiner, M., 2015. Mapping global cropland and field size. Glob. Chang. Biol. 21, 1980–1992. https://doi.org/10.1111/gcb.12838

Fritz, S., McCallum, I., Schill, C., Perger, C., See, L., Schepaschenko, D., van der Velde, M., Kraxner, F., Obersteiner, M., 2012. Geo-Wiki: An online platform for improving global land cover. Environ. Model. Softw. 31, 110–123. https://doi.org/10.1016/J.ENVSOFT.2011.11.015

Funk, C., Peterson, P., Landsfeld, M., Pedreros, D., Verdin, J., Shukla, S., Husak, G., Rowland, J., Harrison, L., Hoell, A., Michaelsen, J., 2015. The climate hazards infrared precipitation with stations—a new environmental record for monitoring extremes. Sci. Data 2, 150066. https://doi.org/10.1038/sdata.2015.66

Gandah, M., Bouma, J., Brouwer, J., Hiernaux, P., Van Duivenbooden, N., 2003. Strategies to optimize allocation of limited nutrients to sandy soils of the Sahel: a case study from Niger, west Africa. Agric. Ecosyst. Environ. 94, 311–319. https://doi.org/10.1016/S0167-8809(02)00035-X

Giuliani, G., Chatenoux, B., De Bono, A., Rodila, D., Richard, J.-P., Allenbach, K., Dao, H., Peduzzi, P., 2017. Building an Earth Observations Data Cube: lessons learned from the Swiss Data Cube (SDC) on generating Analysis Ready Data (ARD). Big Earth Data 1, 100–117. https://doi.org/10.1080/20964471.2017.1398903

Griffiths, P., Nendel, C., Hostert, P., 2019. Intra-annual reflectance composites from Sentinel-2 and Landsat for national-scale crop and land cover mapping. Remote Sens. Environ. 220, 135–151. https://doi.org/10.1016/J.RSE.2018.10.031

Hiernaux, P., Ayantunde, A., Kalilou, A., Mougin, E., Gérard, B., Baup, F., Grippa, M., Djaby, B., 2009. Trends in productivity of crops, fallow and rangelands in Southwest Niger: Impact of land use, management and variable rainfall. J. Hydrol. 375, 65–77. https://doi.org/10.1016/j.jhydrol.2009.01.032

Hiernaux P. and M.D. Turner, 2002. The influence of farmer and pastoralist management practices on desertification processes in the Sahel. In 'Global desertification: do humans cause deserts?' , Reynolds J.F. and D.M. Stafford Smith (eds) Dahlem University Press, Berlin: 135-148.

Huang, H., Chen, Y., Clinton, N., Wang, J., Wang, X., Liu, C., Gong, P., Yang, J., Bai, Y., Zheng, Y., Zhu, Z., 2017. Mapping major land cover dynamics in Beijing using all Landsat images in Google Earth Engine. Remote Sens. Environ. 202, 166–176. https://doi.org/10.1016/j.rse.2017.02.021

Lambert, M.-J., Waldner, F., Defourny, P., Lambert, M.-J., Waldner, F., Defourny, P., 2016. Cropland Mapping over Sahelian and Sudanian Agrosystems: A Knowledge-Based Approach Using PROBA-V Time Series at 100-m. Remote Sens. 8, 232. https://doi.org/10.3390/rs8030232

Leroux, L., Jolivot, A., Bégué, A., Seen, D. Lo, Zoungrana, B., 2014. How Reliable is the MODIS Land Cover Product for Crop Mapping Sub-Saharan Agricultural Landscapes? 8541–8564. https://doi.org/10.3390/rs6098541

Massey, R., Sankey, T.T., Congalton, R.G., Yadav, K., Thenkabail, P.S., Ozdogan, M., Sánchez Meador, A.J., 2017. MODIS phenology-derived, multi-year distribution of conterminous U.S. crop types. Remote Sens. Environ. 198, 490–503. https://doi.org/10.1016/J.RSE.2017.06.033

Mortimore, M., Tiffen, M., Boubacar, Y., Nelson, J., 2001. SYNTHESIS OF LONG-TERM CHANGE IN MARADI DEPARTMENT, NIGER, 1960-2000. Drylands Research Working Paper 39e, Drylands Research, Crewkerne, United Kingdom.

Pekel, J.F., Cottam, A., Gorelick, N., Belward, A.S., 2016. High-resolution mapping of global surface water and its long-term changes. Nature 540, 418–422. https://doi.org/10.1038/nature20584

Pelletier, C., Valero, S., Inglada, J., Champion, N., Dedieu, G., 2016. Assessing the robustness of Random Forests to map land cover with high resolution satellite image time series over large areas. Remote Sens. Environ. 187, 156–168. https://doi.org/10.1016/J.RSE.2016.10.010

Penning de Vries, F.W.T., Djitèye, M.A., 1982. The Productivity of Sahelian Rangeland: a Study of Soils, Vegetation and the Exploitation of This Natural Resource
Centre for Agricultural Publishing and Documentation, Wageningen, The Netherlands: 547.
Pieri C. 1989. Fertilité des terres de savanes: bilan de trente ans de recherche et de développement agricole au sud du Sahara. Ministère de la Coopération, CIRAD-IRAT, Paris, France: 444.

Rasmussen, L.V., Rasmussen, K., Reenberg, A., Proud, S., 2012. A system dynamics approach to land use changes in agro-pastoral systems on the desert margins of Sahel. Agric. Syst. 107, 56–64. https://doi.org/10.1016/j.agsy.2011.12.002

Rasmussen, L.V., Reenberg, A., 2012. Land use rationales in desert fringe agriculture. Appl. Geogr. 34, 595–605. https://doi.org/10.1016/j.apgeog.2012.03.005

Raynaut, C., 1998. Diversité et dynamique des relations sociétés—nature au Sahel. Natures Sci. Sociétés 6, 59–62.

Samaké, O., Smaling, E.M.A., Kropff, M.J., Stomph, T.J., Kodio, A., 2005. Effects of cultivation practices on spatial variation of soil fertility and millet yields in the Sahel of Mali. Agric. Ecosyst. Environ. 109, 335–345. https://doi.org/10.1016/j.agee.2005.02.024

Samasse, K., Hanan, N., Tappan, G., Diallo, Y., Samasse, K., Hanan, N.P., Tappan, G., Diallo, Y., 2018. Assessing Cropland Area in West Africa for Agricultural Yield Analysis. Remote Sens. 10, 1785. https://doi.org/10.3390/rs10111785

Serpantié, G., Ouattara, B., Louppe, D., Sougafara, B., Gnahoua, G.M., Ouattara, N., Kolou, O., Yossi, H., Mallet, B., 2001. Fertilité et jachères en Afrique de l'Ouest. La jachère en Afrique Trop. la jachère Nat. à la jachère améliorée. Le point des connaissances: 21–83.

Schlecht, E., Hiernaux, P., Achard, F., Turner, M.D., 2004. Livestock related nutrient budgets within village territories in western Niger. Nutr. Cycl. Agroecosystems 68, 199–211. https://doi.org/10.1023/B:FRES.0000019453.19364.70

Sheffield, J., Wood, E.F., Chaney, N., Guan, K., Sadri, S., Yuan, X., Olang, L., Amani, A., Ali, A., Demuth, S., Ogallo, L., 2014. A drought monitoring and forecasting system for sub-sahara african water resources and food security. Bull. Am. Meteorol. Soc. 95, 861–882. https://doi.org/10.1175/BAMS-D-12-00124.1

Sultan, B., Roudier, P., Quirion, P., Alhassane, A., Muller, B., Dingkuhn, M., Ciais, P., Guimberteau, M., Traore, S., Baron, C., 2013. Assessing climate change impacts on sorghum and millet yields in the Sudanian and Sahelian savannas of West Africa. Environ. Res. Lett. 8, 014040. https://doi.org/10.1088/1748-9326/8/1/014040

Tappan, G. G., Cushing, W.M., Cotillon, S.E., Mathis, M.L., Hutchinson, J.A., and Dalsted, K.J., 2016, West Africa Land Use Land Cover Time Series: U.S. Geological Survey data release, http://dx.doi.org/10.5066/F73N21JF

Tong, X., Brandt, M., Hiernaux, P., Herrmann, S.M., Tian, F., Prishchepov, A. V., Fensholt, R., 2017. Revisiting the coupling between NDVI trends and cropland changes in the Sahel drylands: A case study in western Niger. Remote Sens. Environ. 191, 286–296. https://doi.org/10.1016/j.rse.2017.01.030

Tony C. Smith and Eibe Frank, 2016 Statistical Genomics: Methods and Protocols, chapter Introducing Machine Learning Concepts with WEKA. Springer, New York, NY: 353-378.

Tsendbazar, N., Herold, M., Fritz, S., Lesiv, M., 2018a. Copernicus Global Land Operations: Validation Report for Moderate Dynamic Land Cover Collection 100m Version 1: Copernicus Global Land Operations. https://land.copernicus.eu/global/sites/cgls.vito.be/files/products/CGLOPS1_VR_LC100m-V1_I1.20.pdf (accessed on 9 October 2019)

Tsendbazar, N.-E., Herold, M., de Bruin, S., Lesiv, M., Fritz, S., Van De Kerchove, R., Buchhorn, M., Duerauer, M., Szantoi, Z., Pekel, J.-F., 2018b. Developing and applying a multi-purpose land cover validation dataset for Africa. Remote Sens. Environ. 219, 298–309. https://doi.org/10.1016/J.RSE.2018.10.025

Turner, M.D., Moumouni, O., 2018. Mosaics of property: control of village land in West Africa. J. Peasant Stud. 1–25. https://doi.org/10.1080/03066150.2018.1439931

van Vliet, N., Reenberg, A., Rasmussen, L.V., Vliet, N. Van, Reenberg, A., Rasmussen, L.V., 2013. Scientific documentation of crop land changes in the Sahel: A half empty box of knowledge to support policy? J. Arid Environ. 95, 1–13. https://doi.org/10.1016/j.jaridenv.2013.03.010

751 Vermote, E.F., El Saleous, N.Z., Justice, C.O., 2002. Atmospheric correction of MODIS data in the visible
752 to middle infrared: first results. Remote Sens. Environ. 83, 97–111. https://doi.org/10.1016/S0034-
753 4257(02)00089-5

754 Wallace, C.S.A., Thenkabail, P., Rodriguez, J.R., Brown, M.K., 2017. Fallow-land Algorithm based on
755 Neighborhood and Temporal Anomalies (FANTA) to map planted *versus* fallowed croplands using MODIS
756 data to assist in drought studies leading to water and food security assessments. GIScience Remote Sens. 54,
757 258–282. https://doi.org/10.1080/15481603.2017.1290913

758 Wu, Z., Thenkabail, P.S., Mueller, R., Zakzeski, A., Melton, F., Johnson, L., Rosevelt, C., Dwyer, J., Jones,
759 J., Verdin, J.P., 2014. Seasonal cultivated and fallow cropland mapping using MODIS-based automated
760 cropland classification algorithm. J. Appl. Remote Sens. 8, 083685. https://doi.org/10.1117/1.JRS.8.083685

761 Xie, H., Tian, Y.Q., Granillo, J.A., Keller, G.R., 2007. Suitable remote sensing method and data for mapping
762 and measuring active crop fields. Int. J. Remote Sens. 28, 395–411.
763 https://doi.org/10.1080/01431160600702673

764 Xiong, J., Thenkabail, P.S., Tilton, J.C., Gumma, M.K., Teluguntla, P., Oliphant, A., Congalton, R.G.,
765 Yadav, K., Gorelick, N., 2017. Nominal 30-m cropland extent map of continental Africa by integrating
766 pixel-based and object-based algorithms using Sentinel-2 and Landsat-8 data on google earth engine. Remote
767 Sens. 9, 1–27. https://doi.org/10.3390/rs9101065

768 Yan, L., Roy, D.P., Zhang, H., Li, J., Huang, H., 2016. An automated approach for sub-pixel registration of
769 Landsat-8 Operational Land Imager (OLI) and Sentinel-2 Multi Spectral Instrument (MSI) imagery. Remote
770 Sens. 8. https://doi.org/10.3390/rs8060520

771 Zhang, W., Brandt, M., Tong, X., Tian, Q., Fensholt, R., 2018. Impacts of the seasonal distribution of
772 rainfall on vegetation productivity across the Sahel. Biogeosciences 15, 319–330. https://doi.org/10.5194/bg-
773 15-319-2018

774 Zhong, L., Hu, L., Yu, L., Gong, P., Biging, G.S., 2016. Automated mapping of soybean and corn using
775 phenology. ISPRS J. Photogramm. Remote Sens. 119, 151–164.
776 https://doi.org/10.1016/j.isprsjprs.2016.05.014

777 Zhong, L., Hu, L., Zhou, H., 2019. Deep learning based multi-temporal crop classification. Remote Sens.
778 Environ. 221, 430–443. https://doi.org/10.1016/J.RSE.2018.11.032

779

780

781

Supplementary material:

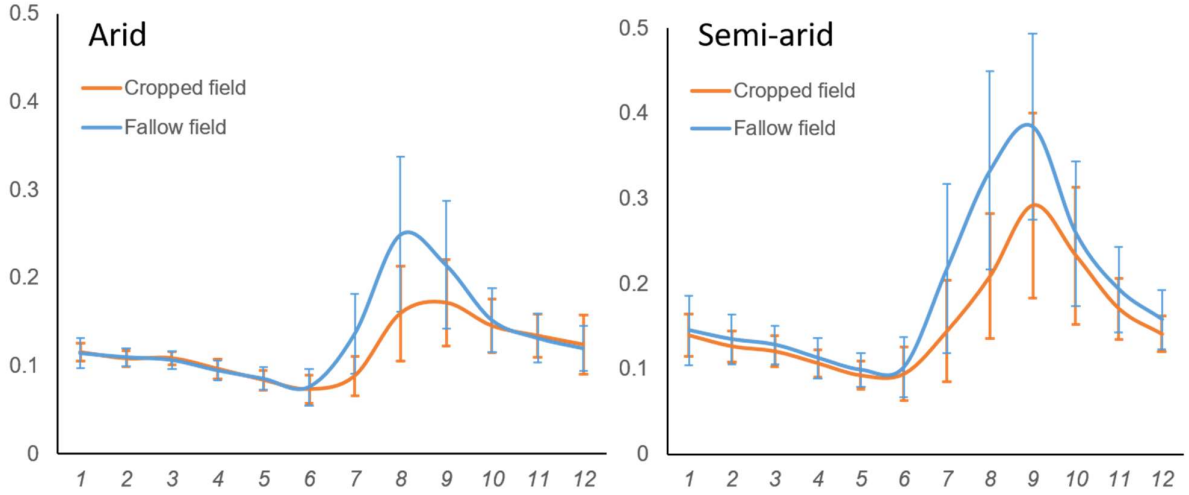

Figure S1. Temporal NDVI profiles of cropped and fallow fields in the arid and semi-arid regime of the Sahel based on average values of sample pixels identified across the study area (see Section 2.3.1) and 95% confidence intervals.

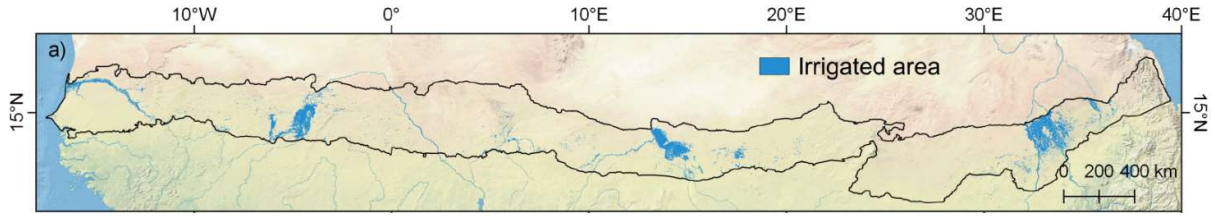

Figure S2. Mask of irrigated areas from the ESA CCI 300 m data.

(http://maps.elie.ucl.ac.be/CCI/viewer/index.php)

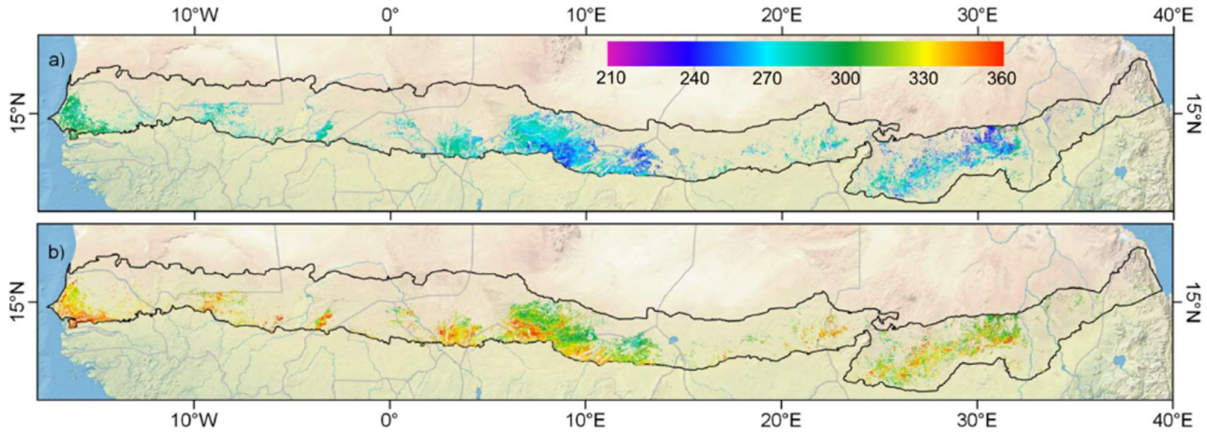

792 Figure S3. MODIS 250 m a) mid of season and b) end of season (day of year) for 2017, within the
793 extent of the CGLS-LC100 cropland class.

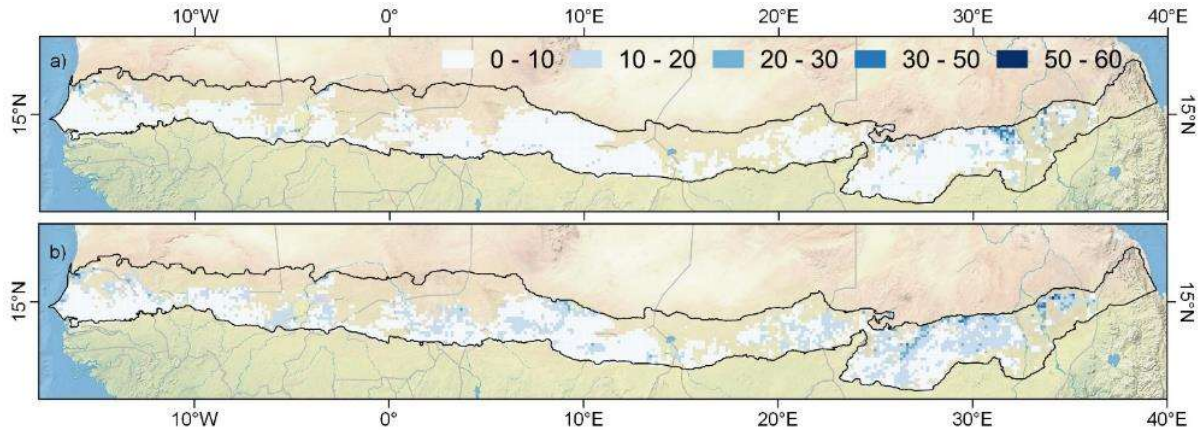

794

795 Figure S4. Standard deviation in number of days for a) start month of image acquisition and b) end
796 month of image acquisition, calculated per grid cell.

797

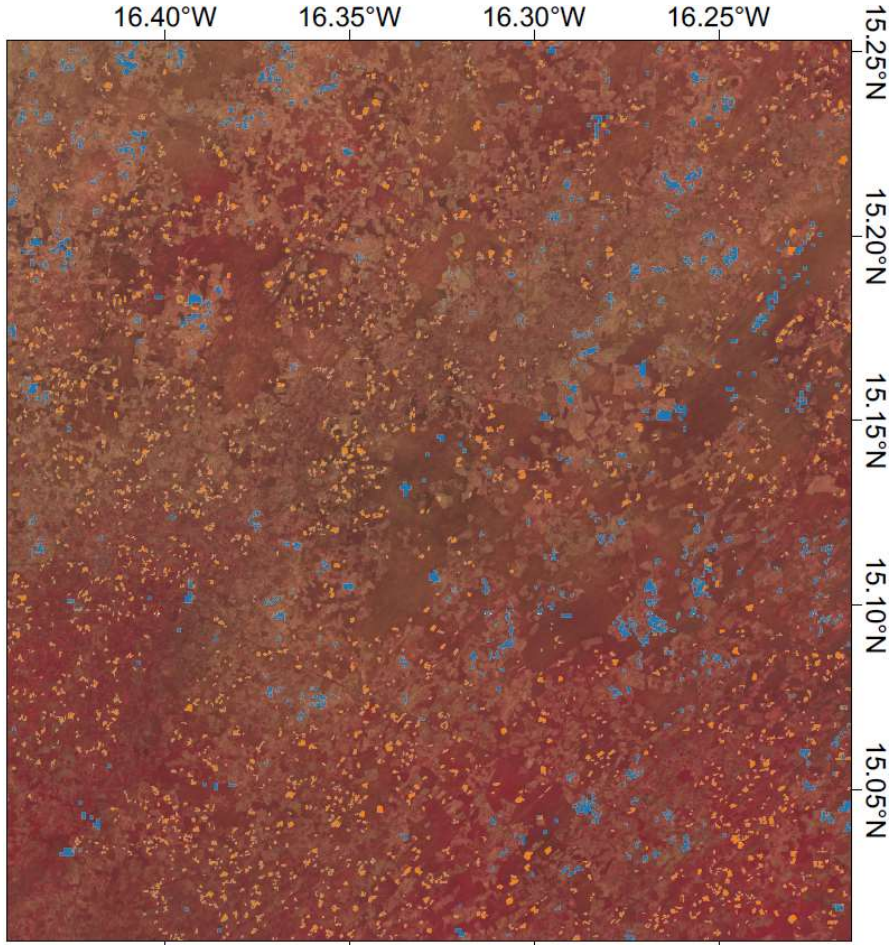

798

Figure S5. Example of the spatial distribution of the final reference data generated in Senegal, covering the same area as Figure 5.

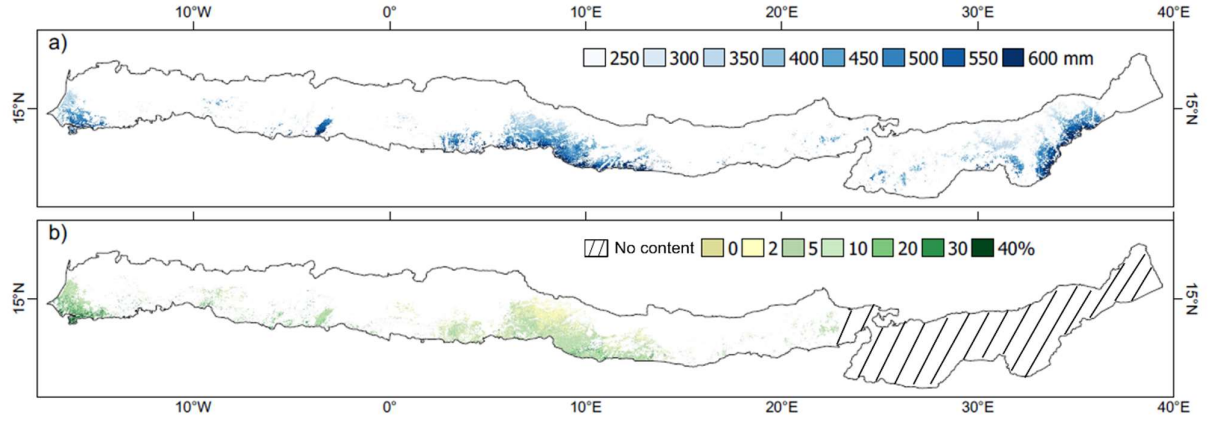

Figure S6. a) CHIRPS annual mean rainfall (1982-2018). b) Woody cover (2014-2016) (Brandt et al., 2018) covering western Sahel, (woody cover for eastern Chad and Sudan was not mapped).

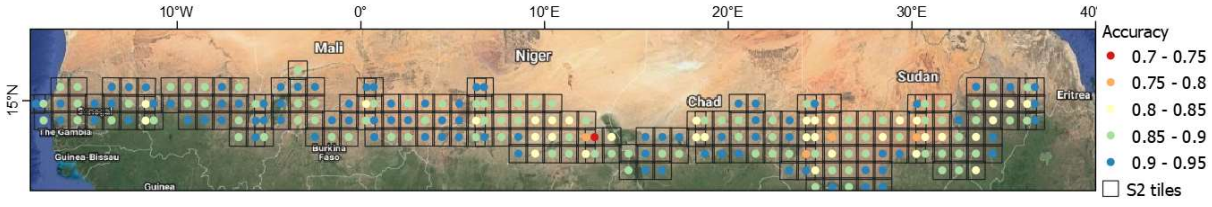

Figure S7. Overall accuracy (OA) of the crop/fallow classification at the Sentinel-2 tile level.

Table S1. Overall accuracy (OA) of the crop/fallow classification at Sentinel-2 tile level.

Name	*OA*	*Name*	*OA*	*Name*	*OA*	*Name*	*OA*	*Name*	*OA*	*Name*	*OA*
27PZS	0.94	29PRS	0.90	31PGQ	0.91	33PWP	0.91	35PKR	0.85	36PVA	0.91
28PBA	0.90	29PRS	0.93	31PGR	0.92	33PWQ	0.91	35PKS	0.94	36PVT	0.86
28PBB	0.90	30PTA	0.92	31PGR	0.91	33PXN	0.92	35PLM	0.92	36PVU	0.86
28PCA	0.91	30PTB	0.91	31PGS	0.91	33PXP	0.86	35PLN	0.86	36PVV	0.87
28PCB	0.91	30PTV	0.90	31PHQ	0.88	33PXQ	0.91	35PLP	0.85	36PWA	0.88
28PCC	0.89	30PUA	0.93	31PHR	0.85	33PYP	0.89	35PLQ	0.80	36PWB	0.90
28PDA	0.89	30PUB	0.94	31PHS	0.87	33PYQ	0.92	35PLR	0.85	36PWC	0.91
28PDB	0.90	30PUC	0.93	31PHT	0.92	33PZQ	0.85	35PLS	0.90	36PWT	0.83

28PDC	0.90	30PVA	0.90	32PKA	0.88	33PZR	0.82	35PMM	0.90	36PWU	0.86
28PEA	0.91	30PVB	0.90	32PKB	0.88	34PBA	0.87	35PMN	0.90	36PWV	0.85
28PEB	0.94	30PVC	0.92	32PKC	0.92	34PBU	0.95	35PMP	0.86	36PXA	0.85
28PFA	0.87	30PWA	0.89	32PKV	0.91	34PBV	0.84	35PMQ	0.87	36PXB	0.82
28PFB	0.93	30PWB	0.87	32PLA	0.87	34PCA	0.86	35PMR	0.88	36PXC	0.89
28PFC	0.94	30PWC	0.91	32PLB	0.90	34PCU	0.92	35PNM	0.92	36PXU	0.91
28PGA	0.91	30PWV	0.94	32PLV	0.88	34PCV	0.91	35PNN	0.93	36PXV	0.93
28PGB	0.90	30PXA	0.93	32PMA	0.87	34PDA	0.90	35PNP	0.89	36PYA	0.90
28PGC	0.91	30PXV	0.90	32PMB	0.90	34PDB	0.92	35PNQ	0.87	36PYB	0.82
28PHA	0.84	30PYA	0.91	32PMU	0.93	34PDU	0.91	35PNR	0.89	36PYC	0.92
28PHB	0.85	30PYB	0.93	32PMV	0.92	34PDV	0.88	35PPM	0.94	36PZA	0.88
28PHC	0.94	30PYV	0.90	32PNA	0.83	34PEA	0.91	35PPN	0.93	36PZB	0.83
29PKR	0.90	30PZA	0.87	32PNB	0.88	34PEB	0.94	35PPP	0.91	36PZC	0.88
29PKS	0.92	30PZB	0.84	32PNU	0.85	34PEU	0.90	35PPQ	0.82	37PBR	0.93
29PLS	0.91	30PZC	0.91	32PNV	0.84	34PEV	0.93	35PPR	0.87	37PBS	0.91
29PLT	0.90	30QVD	0.90	32PPA	0.82	34PFA	0.86	35PQP	0.93	37PBT	0.94
29PMR	0.93	31PBQ	0.92	32PPB	0.87	34PFU	0.90	35PQP	0.90		
29PMS	0.90	31PBR	0.91	32PPU	0.86	34PFV	0.89	35PQQ	0.86		
29PMT	0.89	31PBS	0.86	32PPV	0.84	34PGA	0.92	35PQR	0.81		
29PNR	0.93	31PBT	0.93	32PQA	0.84	34PGT	0.92	35PRP	0.81		
29PNS	0.90	31PCQ	0.90	32PQU	0.87	34PGU	0.90	35PRQ	0.80		
29PNT	0.87	31PCR	0.92	32PQV	0.90	34PGV	0.94	35PRR	0.81		
29PPR	0.93	31PCS	0.93	32PRA	0.90	34PHA	0.83	35PRS	0.91		
29PPS	0.92	31PDQ	0.90	32PRU	0.85	34PHB	0.89	36PTA	0.88		
29PPT	0.94	31PDR	0.92	32PRV	0.80	34PHT	0.91	36PTB	0.90		
29PQQ	0.90	31PDS	0.89	33PTP	0.86	34PHT	0.79	36PTU	0.89		
29PQR	0.90	31PEQ	0.94	33PTQ	0.73	34PHU	0.80	36PTV	0.85		
29PQS	0.91	31PER	0.90	33PUP	0.87	34PHV	0.84	36PUA	0.88		
29PQT	0.90	31PES	0.91	33PUQ	0.84	35PKM	0.88	36PUB	0.90		
29PRQ	0.91	31PFQ	0.92	33PVN	0.90	35PKN	0.84	36PUT	0.87		
29PRR	0.91	31PFR	0.93	33PVP	0.90	35PKP	0.88	36PUU	0.87		

	31PFS	0.90	33PWN	0.93	35PKQ	0.84	36PUV	0.83

809